PHOTOELECTRONICS

UDC 621. PACS: 85, 85.60.–q
EDN: AYVMCY

Uncooled 640×512 photosensor array for the spectral range of 0.4–2.0 μm from colloidal quantum dots PbS with a hole transport layer based on *p*-PbS-EDT CQDs

V. P. Ponomarenko, V. S. Popov, M. A. Pankov, K. A. Khamidullin, A. D. Deomidov, A. A. Fedorov, G. Yu. Deev, D. E. Dragunov, O. V. Epifanov, P. S. Lazarev, E. V. Mirofyanchenko, D. V. Ilyinov, V. A. Petrushina, I. D. Burlakov, A. V. Polessky, V. V. Startsev, S. B. Brichkin, M. G. Spirin, S. A. Tovstun, M. V. Gapanovich, V. Yu. Gak, A. V. Gadomskaya, D. N. Pevtsov, A. V. Katsaba, A. S. Kirichenko, D. V. Dyomkin, V. A. Ivanova, V. V. Ivanov, V. F. Razumov

The architecture and main characteristics of the 640×512 photosensor array (15 μm pitch) with spectral range sensitivity of 0.4–2.0 μm developed on the basis of PbS colloidal quantum dots are presented. The layer for generating the main fraction of photocarriers is made on the basis of n-PbS CQDs by replacing the initial ligand (oleic acid) with iodine during the treatment of the CQD layer with tetra-n-butylammonium iodide (TBAI). Transport layers for electrons and holes were produced based on n-ZnO and p-PbS EDT CQDs, where the hole transport layer of p-PbS-EDT CQDs was created by replacing the initial ligand by treating the CQD layer with ethane-1,2-dithiol (EDT).

Keywords: colloidal quantum dot; photosensor; ligand; photosensitivity.

DOI: 10.51368/1996-0948-2025-1-45-54

1. Introduction

The unique properties of low dimensional semiconductor structures increasingly attract attention of researchers in such fields as photonics, biomedicine, microelectronics, etc. Recently, the progress reached with the use of quasi-zero-dimensional quantum dots in the creation of solar energy devices [1], biomarkers [2], focal plane arrays (FPA) [3], lasers [4], etc., is particularly noticeable.

Currently, there are two companies leading the industrial production of optoelectronics using colloidal quantum dots: SWIR Vision (USA) and Quantum Solutions (UK), which mass-produce wide-spectrum full-format photosensors array and night video cameras based on them with a photosensitivity range from 0.4 to 2.0 μm, manufactured using hybrid-monolithic technology. In 2020, SWIR Vision demonstrated uncooled 640×512, 1280×1024, and 1920×1080 FPA, on lead sulfide colloidal quantum dots with a photosensitive element (PSE) pitch of 15 μm. Currently, the company's product line includes 5 types of photosensor arrays, including 2040×2040 and 3064×2040 photosensors of the with a

PSE pitch of 7 μm. In 2024, Quantum Solutions introduced a 640×512 FPA made of lead sulfide colloidal quantum dots with the smallest pitch of 5 μm achieved to date in industrial samples of IR FPA. Both companies produce compact night vision cameras using self-engineered FPAs made from colloidal quantum dots.

Previously, in [5], we described a single-element photosensor developed by us for the spectral range of 0.4–2.0 μm, made of colloidal PbS nanoparticles on a Si/SiO_2 substrate with the architecture shown in Figure 1*a*. Small-sized 12×12 μm photosensitive elements of diode type with an energy barrier of the *p–n* junction type at the contact of layers of colloidal quantum dots (CQD) of lead sulfide (PbS) of *n*- and *p*-type conductivity were studied. The *p–n* junction type energy barrier was obtained by modifying the CQD surface with appropriate ligands. The PbS CQD layer of the electron conductivity type (*n*-type) was created by replacing the initial ligand used in the synthesis of CQDs (*oleic acid* $C_{18}H_{34}O_2$) with iodine (I) by treating the PbS CQD layer with *tetra-n-butylammonium iodide* $[(C_4H_9)_4N]I$ (TBAI). Similarly, a *p*-type PbS CQD layer was created by replacing the original ligand after treating the PbS CQD layer with *ethane-1,2-dithiol* $C_2H_6S_2$ (EDT). The absorption of radiation from the spectral interval of 0.4–2.0 μm was mainly performed by the *n*-PbS-TBAI CQD electronic conduction type layer due to its significantly greater thickness compared to the *p*-PbS-EDT CQD layer. The *p*-PbS-EDT CQD layer was used as an electron blocking layer near the anode of the photosensitive structure and, at the same time, served as a hole transport channel.

The PbS CQD for I- and *p*-type conductivity layers had a diameter of 7.6 nm and 3.1 nm, respectively, which created an additional energy heterobarrier at the contact of these layers, facilitating the efficient separation of photocarriers formed after the decay of photoexcitons in the *n*-PbS-TBAI CQD layer. *Lead chloride* ($PbCl_2$) was used as the lead precursor and *N,N′-diphenylthiourea* ($SC(NHPh)_2$) was used as the sulfur precursor. A layer of *n*-ZnO nanoparticles with electron conductivity served as a layer for blocking the flow of holes in the area near the cathode and, at the same time, as a channel for transporting electrons to the cathode. The upper radiation-transparent electrode was created by aerosol printing of a layer based on silver nanowires (AgNW), with an optical transmittance in the wavelength range of 0.4–2.0 μm of about 65–70 % and high conductivity [6], which sets them apart from conductive coatings made of carbon nanowires or ITO $(In_2O_3)_{0.9}$-$(SnO_2)_{0.1}$ (see Fig. 1*b*). Thus, the architecture of the photosensors developed in [5] had the form Cr/Ni/*n*-ZnO/*n*-PbS-TBAI CQD/*p*-PbS-EDT CQD/AgNW. The energy structure of the individual layers of this structure is shown in Figure 2.

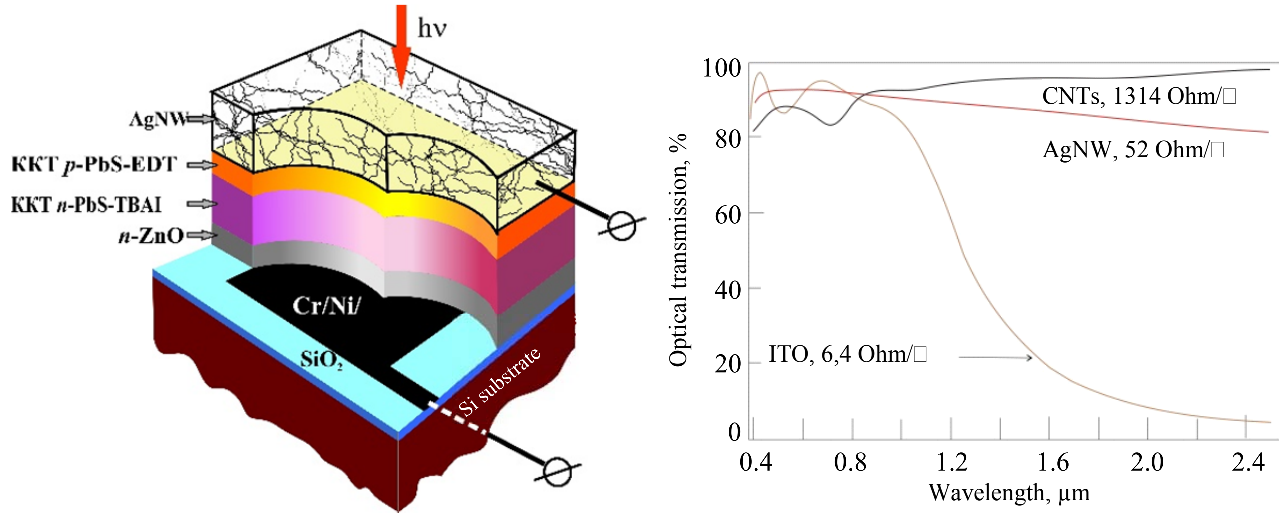

a) *b)*

Fig. 1 Single-element photosensor based on colloidal quantum dots PbS CQD with transport layers for electrons and holes made of n-ZnO nanoparticles and p-PbS-EDT CQD, respectively: a) – photosensor architecture [5]; b) – optical transmittance and specific resistance of layers of carbon nanotubes (CNTs), silver nanowires (AgNWs) and coatings of $(In_2O_3)_{0.9}$-$(SnO_2)_{0.1}$ (ITO) [6]

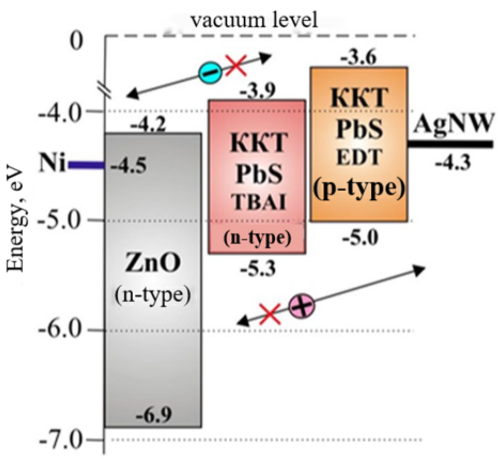

Fig. 2 Energy structure of layers of the Cr/Ni/n-ZnO/CQDn-PbS-TBAI/CQDp-PbS-EDT/AgNW structure, on the basis of which a single-element photosensor is manufactured [5]

The spectral dependence of the relative sensitivity of the sensor is shown in Figure 3*a*. The current-voltage characteristics (CVC) curves of the photosensors had a shape typical for semiconductor structures with an energy barrier and differential resistance of the dark CVC at zero bias, lying within the range of $(2–20)\times10^{10}$ Ohm. The values of specific detectability of $(2–4)\times10^{12}$ cm·Hz$^{1/2}$·W^{-1} (Fig. 3*b*) were achieved when the photosensor was illuminated by radiation from a blackbody with a temperature of 1273 K.

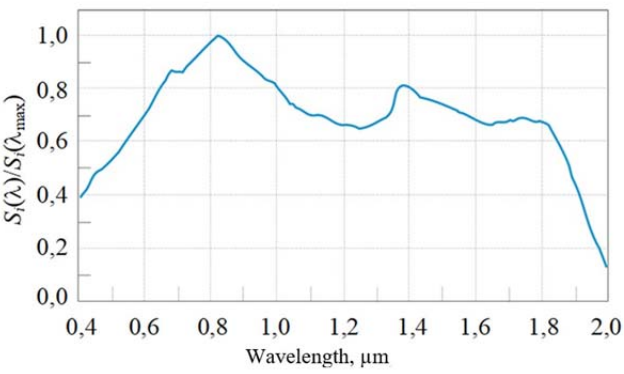

Fig. 3 Spectral dependences of the relative photosensitivity (a) [5] and specific detectability (b) of a single-element photosensor based on colloidal PbS quantum dots with the Cr/Ni/n-ZnO/CQD n-PbS-TBAI/CQD p-PbS-EDT/AgNW architecture

2. Architecture of the 640×512 photosensor array

In this paper, we describe a new FPA developed by us for the spectral range of 0.4–2.0 µm in the 640×512 format with a photosensitive elements pitch of 15 µm, made of colloidal quantum dots PbS CQD on the surface of a silicon ROIC for reading p-channel photo signals. The architecture of this MPD is shown in Figure 4.

The production of this FPA is based on the direct formation of a photosensitive structure on the surface of a silicon readout integrated circuit (ROIC). The photosensitive and functional layers of the sensor are produced by successive applying pre-synthesized liquid suspensions of nanoparticles with a given composition and viscosity using the spin-coating technique or the aerosol printing method. This ensures the production of a monolithic structure without the use of indium or other microcontacts, which are typical for the classical technology of hybridization (combining) of photodiodes or photoresistors array based on layers of bulk or epitaxial 3D semiconductor materials with microelectronics for reading photo signals. This technology for manufacturing photosensors, called hybrid-monolithic, is described in general terms in [3, 5, 7–9]. It ensures the removal of critically important restrictions on the pitch of sensitive elements, as a result of which the pitch is limited only by the diffraction limit and the pitch of the ROIC, which is determined by the circuitry of the readout cell and the topological norm of the CMOS technology by which the silicon ROIC is manufactured.

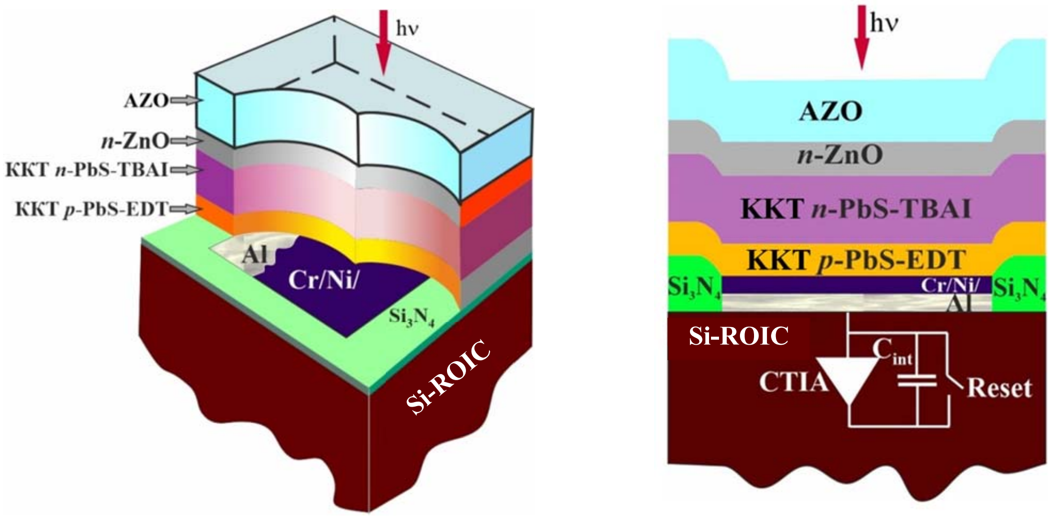

Fig. 4 640×512 photosensor array based on PbS CQD with transport layers for holes and electrons from p-PbS-EDT and n-ZnO CQD, respectively: a) – photosensor architecture; b) – cross-section of the photosensitive element with the input device of the silicon ROIC readout cell (CTIA – transimpedance amplifier, Reset – reset key, C_{int} – photo signal accumulation capacitance)

The architecture of each photosensitive element developed by the authors of the new PbS CQD based 640×512 photosensor array has the form Cr/Ni/*p*-PbS-EDT CQD/*n*-PbS-TBAI CQD/*n*-ZnO/AZO. The energy structure of individual layers demonstrating the directions of electron and hole transport in the layers of the photosensor is shown in Figure 5.

As in the case of the single-element photosensor [5] described above, the main proportion of photocarriers is generated by radiation in the *n*-PbS-TBAI CQD layer. After the decay of photoexcitons, electrons and holes are separated by an energy barrier of the *p–n* junction type at the contact of the *n*-PbS-TBAI CQD and *p*-PbS-EDT CQD layers. The *n*-ZnO and *p*-PbS-EDT CQD layers serve to block holes and electrons in the regions located near the anode and cathode. They are also channels for transporting electrons and holes.

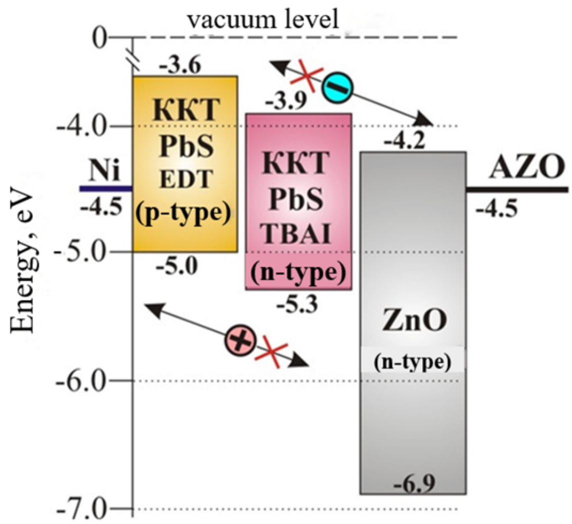

Fig. 5 Energy structure of layers of the Cr/Ni/p-PbS-EDT CQD/n-PbS-TBAI CQD/n-ZnO/AZO structure, on the basis of which the 640×512 photosensor array is made, demonstrating the directions of electron and hole transport

Manufacturing of PbS CQD layers of electronic and hole conductivity types is carried out by replacing the initial ligand (oleic acid) after treatment with *tetra-n-butylammonium iodide* (*n*-type) and *ethane-1,2-dithiol* (*p*-type). As in work [5], *lead chloride* and *N,N'-diphenylthiourea* are used as precursors of lead and sulfur in the synthesis of PbS CQD. In addition, in contrast to the above-described single-element photosensor with the Cr/Ni/n-ZnO/*n*-PbS-TBAI CQD/*p*-PbS-EDT CQD/AgNW architecture, here, instead of a layer based on AgNW nanowires, we used a coating of zinc oxide doped with aluminum to form a solid solution in the ZnO-Al_2O_3 (AZO) system as a radiation-transparent electrode [10]. A photograph of the manufactured 640×512 photosensitive element array based on PbS CQD with a silicon ROIC for reading and pre-processing photo signals and an upper electrode made of Al:ZnO (AZO), mounted on a raster for research, is shown in Figure 6.

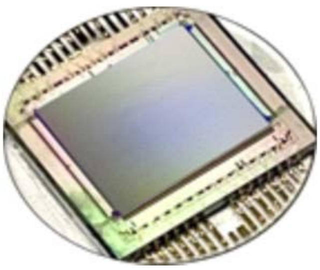

Fig. 6 Photograph of a 640×512 photosensitive element array with a ROIC on a raster

3. Properties of a 640×512 photosensor array with a hole transport layer based on *p*-PbS-EDT CQD

High-resolution transmission electron microscopy (TEM) was used to control the size of the synthesized colloidal quantum dots. The spectral dependences of the optical absorption of a suspension of colloidal quantum dots of lead sulfide in a solution of *n-octane*, synthesized by the above-described method using $PbCl_2$ as a lead precursor, were studied. The first exciton absorption peak was observed with a maximum located at a $\lambda_{max} \approx 1{,}85$ μm wavelength. Its full width at half maximum (FWHM) was 220 nm, which indicates a sufficiently high monodispersity of PbS nanocrystals in the absorbing layer of *n*-PbS-TBAI CQD. Figure 7 shows the spectral dependence of the photosensitivity $S_i(\lambda)/S_i(\lambda_{max})$ reduced to unity for the manufactured 640×512 matrix photosensor with a silicon integrated circuit for reading and pre-processing photo signals.

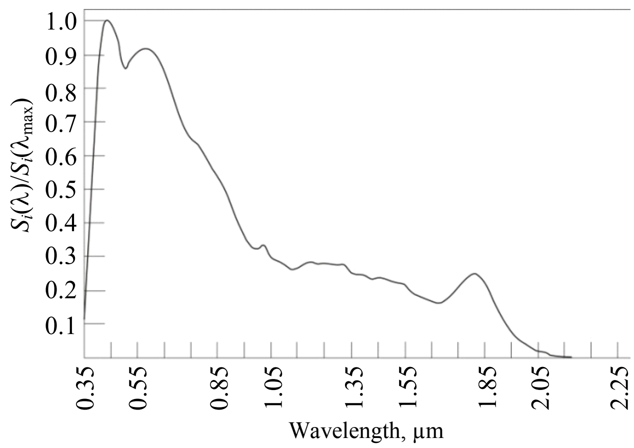

Fig. 7 Spectral dependence of photosensitivity at room temperature reduced to unity for a 640×512 photosensor array with a silicon ROIC for reading and pre-processing photo signals

The use of the empirical relationship $E_0 = 0.41 + (0.025d^2 + 0.283d)^{-1}$ that establishes the connection between the energy of optical transitions E0 in the optical absorption spectra of the CQD solution and the diameter *d* of the nanoparticles, obtained in [11], showed that the diameter of the colloidal quantum dots we used is $d \simeq 9.5$–10 nm. A study of the shape of the nanoparticles using high-resolution transmission electron microscopy showed that it is close to a truncated octahedron. Each colloidal quantum dot has eight faces (111) and six faces (100).

Figure 8 shows fragments of images of fan blades and a human face obtained in the daytime at an illumination of the observed scene of 300–500 lux using a 640×512 photosensor array (15 μm pitch). Single-point correction and signal calibration using a defocused image were used.

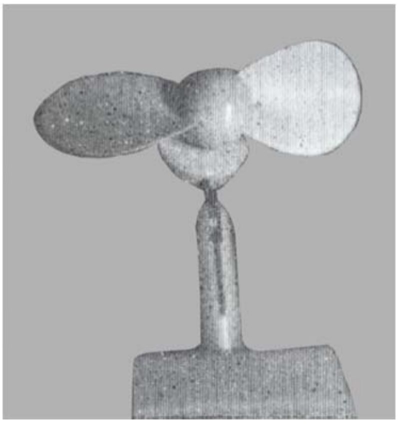

a)

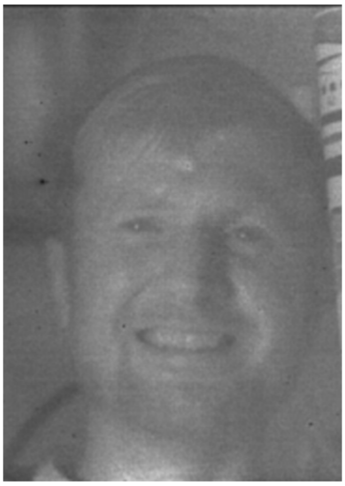

b)

***Fig. 8** Image fragments obtained using an uncooled 640×512 (15 μm pitch) photosensor array based on PbS colloidal quantum dots for the spectral range of 0.4–2.0 μm with the Cr/Ni/p-PbS-EDT QCD/n-PbS-TBAI QCD/n-ZnO/AZO architecture*

4. Conclusion

One of the areas of improvement of night vision devices (NVD) is the expansion of their spectral sensitivity areas. The sensitivity of modern mass-produced electro-optical converters (EOCs), including 3+ generation with photocathodes based on gallium arsenide with negative electron affinity, is limited to a spectral range of 0.4–0.9 μm. This results in a number of drawbacks of modern night vision devices, due to which the requirements for range, probability of detection and identification may not be met. The main one is the insufficient range of vision of the night vision devices at night illumination of the observed scene below 2×10^{-3} lux. This type of illumination is typical for objects located in mountain gorges, tunnels, on unlit city streets, under the forest canopy, etc. It is caused by diffuse or direct light from the moon, stars, zodiacal light, the proper radiation of the upper layers of the atmosphere associated with the recombination of ions formed during the day, etc. Figure 9*a* shows the spectral dependence of the power density of natural night illumination (NNI) on a vertical surface [12].

It is evident that the illumination level increases significantly in the wavelength range of $\Delta\lambda$ = 0.4–1.8 μm compared to the range of $\Delta\lambda$ = 0.4–0.9 μm typical for modern mass produced EOCs. Thus, the average value of NNI in the absence of the moon in the wavelength range of 0.6–0.8 μm in clear weather (snow background) is $(1.5–3.0)\times10^{-5}$ W/m^2·μm, while in the range of 1.4–1.8 μm, even with continuous cloud cover (green background), it increases to $(6.0–7.0)\times10^{-4}$ W/m^2·μm. The source of illumination here is the radiation of atmospheric oxygen. Along with the increase in illumination, a significant gain in optical transmission of the atmosphere occurs when moving from the spectral region of 0.4–0.9 μm to the region of 0.4–1.8 μm (Fig. 9*b*). The attenuation of the luminous flux by the atmosphere is associated with the absorption of light by water vapor and carbon dioxide and scattering by fluctuations in the density of the gaseous medium of the atmosphere and by various solid dust particles. The assessment carried out in [13] showed that with a meteorological viewing range of $S_M = 10$ km, the transmittance of 1 km thick atmospheric layer at a wavelength of $\lambda = 0.6$ µm is 0.72, and in the center of the transparency window of 1.4–1.8 µm it increases to a value of 0.93.

Photosensors array based on epitaxial $In_{053}Ga_{047}As$ with an InP substrate, which technology has developed increasingly, easily implement a long-wave photosensitivity limit of $\lambda_{co} \cong 1.6$ µm. However, to ensure sensitivity in the visible range, their production requires the use of special technological operations to thin the InP substrate after hybridization with the ROIC [14] for photo signal reading. The remaining InP layer, which is approximately 0.2 µm thick, still limits the quantum efficiency of the photosensor in the visible range to ≤ 60 %. The need to use indium or copper microcontacts for hybridization of the photosensitive elements (PSE) array made of InGaAs with Si ROIC–limits the minimum step of the PSE to a value of about 5 µm.

CQD matrices adopt frontal illumination and no substrates that limit photosensitivity in the visible range of electromagnetic radiation. Also, no metal microcontacts are required for hybridization of the photosensitive elements array with the Si ROIC. The use of hybrid-monolithic manufacturing methods [7] allows to create wide-spectrum matrices based on CQD with a 0.4–2.0 µm sensitivity range and a pitch of photosensitive elements limited only by the diffraction limit of the recorded radiation, the circuitry of the reading cell, and the topological norm of the CMOS technology, according to which the Si ROIC is manufactured.

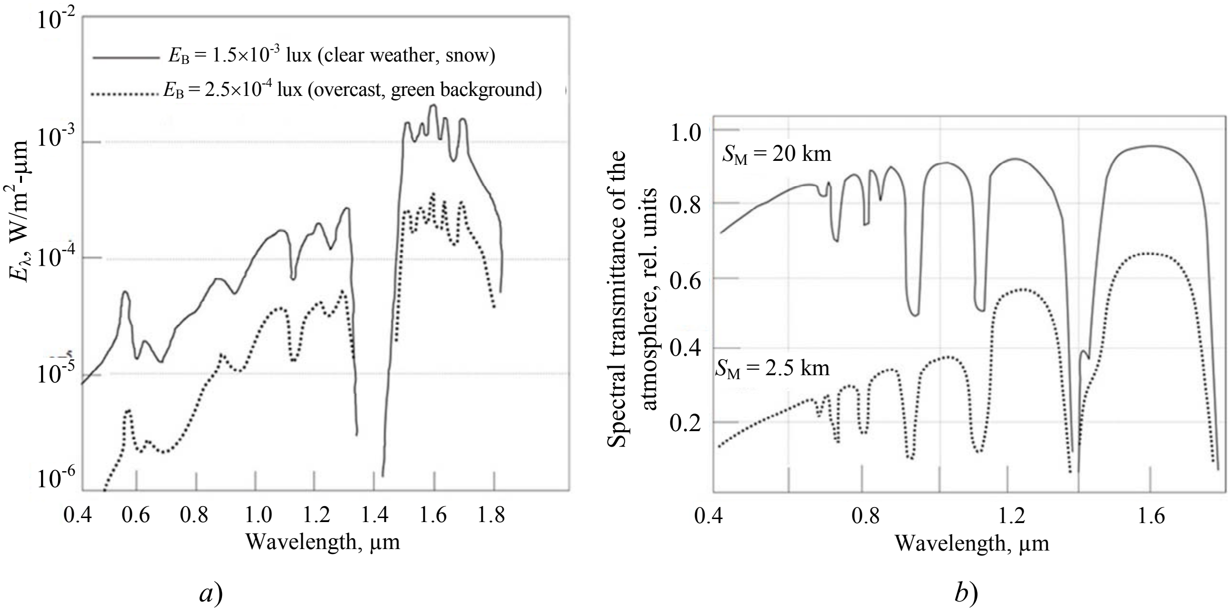

Fig. 9. a) – spectral dependence of the power density of natural night illumination on the vertical surface E_B under conditions of continuous cloudiness (green background), and for the case of clear weather against the background of a surface covered with snow; b) – spectral dependence of the transmission of an atmospheric layer 1 km thick for cases of meteorological vision range S_M = 20 km and S_M = 2.5 km [12]

This work was supported by the Advanced Research Foundation.

REFERENCES

1. You H. R., Park J. Y., Lee D. H., Kim Y. and Choi J., Appl. Sci. **10**, 975 (2020). https://doi.org/ 10.3390/app10030975

2. Panja A. and Patra P., Inorganic Nanoparticle Luminphore: Design and Application **6** (4) (2023). https://doi.org/10.1051/fopen/2022020

3. Ponomarenko V. P., Popov V. S., Shuklov I. A., Ivanov V. V. and Razumov V. F., Russ. Chem. Rev. **93** (4), RCR 5113 (2024). https://doi.org/10.59761/RCR5113

4. Wang Y. and Sun H., Progress in Quantum Electronics **60**, 1 (2018). https://doi.org/10.1016/j.pquantelec.2018.05.002

5. Popov V. S., Ponomarenko V. P., Dymkin D. V., Shuklov I. A., Gadomska A. V., Brichkin S. B., Lavrentiev N. A., Gak V. U., Mirofyanchenko A. E., Mirofyanchenko E. V., Katsaba A. V., Arsenov P. V., Corresponding Member of the RAS Ivanov V. V. and Corresponding Member of the RAS Razumov V. F., Doklady Physics **68** (7), 233–236 (2023). https://doi.org/10.31857/S2686740023040120

6. Langley D., Giusti G., Mayousse C., Celle C., Bellet D. and Simonato J.-P., Nanotechnology **24** (45), 452001 (2013). https://doi.org/10.1088/0957-4484/24/45/452001

7. Popov V. S., Ponomarenko V. P. and Popov S. V., Journal of Communications Technology and Electronics **69** (4–6), 219–226 (2024). https://doi.org/ 10.51368/1996-0948-2023-6-45-53

8. Malinowski P. E., Georgitzikis E., Maes J., Vamvaka I., Frazzica F., Van Olmen J., De Moor P., Heremans P., Hens Z. and Cheyns D., Sensors **17**, 2867 (2017). https://doi.org/10.3390/s17122867

9. Klem E. J. D., Lewis J., Gregory C., Cunningham G. and Temple D., Proc. of SPIE **8353**, 835337 (2012).

10. Ajili M., Jebbari N., Turki N. K. and Castagné M., International Renewable Energy Congress (IREC2010, November 5–7, Tunisia), pp. 305–310.

11. Moreels I., Lambert K., Smeets D., De Muynck D., Nollet T., Martins J. C., Vanhaecke F., Vantomme A., Delerue C., Allan G. and Hens Z., ACS Nano **3** (10), 3023–3030 (2009). https://doi.org/ 10.1021/nn900863a

12. Gusarova N. I., Koshchavtsev N. F. and Popov S. V., J. Commun. Technol. **61** (10), 1211–1214 (2016). https://doi.org/10.1134/S1064226916100144

13. Koshchavtsev N. F., Koshchavtsev A. N. and Fedotova S. F., Applied Physics, No. 3, 66–69 (1999) [in Russian].

14. Burlakov I. D., Grinchenko L. Y., Dirochka A. I. and Zaletaev N. B., Advances in Applied Physics **2** (2), 131–136 (2014) [in Russian].

Vladimir P. Ponomarenko[1,2], Chief Designer, Head of the Department, Doctor of Physical and Mathematical Sciences, Professor
Viktor S. Popov[1,2], Head of the Center, Head of the Laboratory, Associate Professor, Candidate of Chemical Sciences
E-mail: popov.vs@mipt.ru
Mikhail A. Pankov[1], Head of Laboratory, Candidate of Physical and Mathematical Sciences
Kamil A. Khamidullin[1], Group Leader, Head of the Department
Aleksandr D. Deomidov[1], Lead Engineer
Artem A. Fedorov[1], Engineer of the 2nd Category
German Yu. Deev[1], Engineer of the 2nd Category
Denis E. Dragunov[1], Engineer of the 1st Category
Oleg V. Epifanov[1], Lead Engineer
Pavel S. Lazarev[1], Lead Engineer
Ekaterina V. Mirofyanchenko[1], Group Leader, Candidate of Technical Sciences
Denis V. Ilyinov[1], Engineer of the 1st Category
Viktoriya A. Petrushina[1], Process Engineer
Igor D. Burlakov[1], Deputy Director General for Innovations and Science, Doctor of Technical Sciences, Professor
Alexey V. Polessky[1], Chief Designer for Research and Development, andidate of Technical Sciences

Vadim V. Startsev[1], Director General, Candidate of Technical Sciences
Sergey B. Brichkin[2,3], Head of the Department, Chief Researcher, Candidate of Chemical Sciences
Maksim G. Spirin[2,3], Senior Staff Scientist, Senior Research Scientist, Candidate of Chemical Sciences
Sergey A. Tovstun[2,3], Senior Staff Scientist, Candidate of Physical and Mathematical Sciences, Associate Professor
Mikhail V. Gapanovich[2,3], Senior Staff Scientist, Candidate of Chemical Sciences
Vladimir Yu. Gak[2,3], Staff Scientist
Anna V. Gadomskaya[2,3], Staff Scientist, Candidate of Chemical Sciences
Dmitry N. Pevtsov[2,3], Process Engineer, Junior Staff Scientist
Alexey V. Katsaba[2], Senior Staff Scientist – Deputy Head of the Laboratory, Candidate of Physical and Mathematical Sciences
Alexey S. Kirichenko[2], Senior Staff Scientist, Candidate of Physical and Mathematical Sciences
Dmitry V. Dyomkin[2], Junior Staff Scientist
Valeriya A. Ivanova[2], Staff Scientist, Candidate of Physical and Mathematical Sciences
Viktor V. Ivanov[2], Director of the Institute of Quantum Technologies of Moscow Institute of Physics and Technology, Doctor of Physical and Mathematical Sciences, Corresponding Member of the Russian Academy of Sciences
Vladimir F. Razumov[2,3], Chief Staff Scientist – Head of the Laboratory, Doctor of Physical and Mathematical Sciences, Professor, Corresponding Member of the Russian Academy of Sciences
[1] RD&P Center ORION, join-stock company
9, Kosinskaya st., Moscow, 111538 Russia
[2] Moscow Institute of Physics and Technology
9, Institutskiy lane, Dolgoprudny, Moscow region, 141701 Russia
[3] Federal Research Center of Problems of Chemical Physics and Medicinal Chemistry RAS
1, Academika Semenova Ave., Chernogolovka, Moscow region, 142432 Russia

Received January 9, 2025
Revised February 6, 2025
Accepted February 10, 2025
Scientific specialty code: 1.3.11